Received September 18, 2017, accepted October 11, 2017, date of publication October 16, 2017,
date of current version November 7, 2017.

Digital Object Identifier 10.1109/ACCESS.2017.2763421

Sub-Nyquist Sampling and Recovery of Pulse Streams With the Real Parts of Fourier Coefficients

NING FU, (Member, IEEE), GUOXING HUANG, LIYAN QIAO, (Member, IEEE), AND HAORAN ZHAO

Department of Automatic Test and Control, Harbin Institute of Technology, Harbin 150080, China

Corresponding author: Liyan Qiao (qiaoliyan@163.com)

This work was supported by the National Natural Science Foundation of China under Grant 61102148 and Grant 61671177.

ABSTRACT We consider the problem of sampling pulse streams with known shapes. The recent finite rate of innovation (FRI) framework has shown that such signals can be sampled with perfect reconstruction at their rate of innovation, which is usually much lower than the Nyquist rate. Although FRI sampling of pulse streams was treated in various works, either the work was unstable for high rate of innovation, or the sampling stage was complex and redundant. In this paper, we propose an FRI sampling and recovery method for pulse streams, which is based on the real parts of the Fourier coefficients. The proposed method is simple and efficient, and leads to stable recovery even when the rate of innovation is very high. This is achieved through modulating the input signal in each channel with a properly chosen cosine signal, followed by filtering with a low-pass filter. Since the modulating process will lead to the signal spectrum aliasing, we propose a spectrum de-aliasing algorithm to solve this problem, resulting in the real parts of a band of Fourier coefficients from each two channels. Combining with the multi-channel sampling structure, we propose a more efficient way to obtain arbitrary frequency bands from the aliased spectrum, which improves the utility of the signal spectrum. By using a sparsity-based recovery algorithm, the time delays and amplitudes of the pulse streams can be recovered from the obtained real parts of the Fourier coefficients. Finally, simulation results have shown that the proposed scheme is flexible and exhibits better noise robustness than previous approaches.

INDEX TERMS Pulse streams, sub-Nyquist sampling, finite rate of innovation (FRI), Fourier coefficients, multi-channel.

I. INTRODUCTION

The well known Shannon-Nyquist theorem states that in order to perfectly reconstruct an analog signal from its samples, it must be sampled at the Nyquist rate, *i.e.,* twice its highest frequency [1]. This assumption is required when the only knowledge on the signal is that it is bandlimited. However, other prior knowledge on the signal, rather than band limitation, can be exploited in order to reduce the sampling rate. A specific prior was explored by Vetterli *et al.* [2], Maravic and Vetterli [3], and Blu *et al.* [4], who considered signals consisting of a stream of short pulses, where the pulse shape is known. Such signals are prevalent in applications such as wireless communication [5]–[7], bio-imaging [8], [9] and radar [10], [11]. These parametric signals have a finite number of degrees of freedom per unit time, also known as the finite rate of innovation (FRI) property. The rate of innovation is the average number of degrees of freedom per unit of time. It was shown that, by using an adequate sampling kernel and a sampling rate greater or equal to the rate of innovation, it is possible to reconstruct such signals uniquely. The FRI framework treats sampling and recovery of signals characterized by a finite number of degrees of freedom per unit time. For such models, the goal is to design a sampling scheme operating at the innovation rate, which is the minimal possible rate from which perfect recovery is possible [12]–[14]. In many cases the FRI sampling rate is much lower than the Nyquist rate.

Following this point of view, various single channel sampling methods were proposed based on Gaussian kernels [2] or polynomial and exponential reproducing kernels [15], [16].

However, these methods are instable for a large number of pulses per unit time. As mentioned in [3], Gaussian kernels are unstable when the pulse number is larger than 6. The authors in [17] also show that the polynomial and exponential reproducing kernels are unstable when the pulse number is larger than 5. In [2], the authors proposed Sinc sampling kernel, *i.e.,* ideal low-pass filter (LPF), to obtain the Fourier coefficients. They showed that the time delays and amplitudes of the pulse streams can be recovered from a set of the signal's Fourier coefficients. However, using a LPF can only extract a consecutive set of Fourier coefficients, which would lead to a poor recovery performance. To extract arbitrary sets of Fourier coefficients, Tur *et al.* [17] introduced a pre-sampling filtering scheme. Such sampling kernel required multiple pass-bands and extremely high frequency selectivity, which are difficult to satisfy when designing a practical analog filter.

Above methods are composed of a single sampling channel. Multichannel sampling schemes offer additional degrees of freedom which can be utilized to achieve the rate of innovation. The work in [18] was the first to address multi-channel sampling scheme to obtain discrete Fourier coefficients distributed over a larger part of the signal's spectrum. They suggest the use of multi-channel mixers and integrators to directly compute and sample the Fourier coefficients. In this method, one channel can only obtain one Fourier coefficient. Implementing this kind of multi-channel circuits in hardware results in a complicated system, characterized by high number of components and large physical dimensions. Another multi-channel sampling scheme was proposed in [19]–[21] to sample distinct bands of the Fourier coefficients. However, in order to avoid spectrum aliasing, this approach samples a band of Fourier coefficients through a complex and redundant way, in which the desired band is modulated to the pass-band of a BPF and then, after filtering, is demodulated to the baseband. In [22] we have proposed a simplified FRI sampling system for pulse streams, based on constraint random modulation. It present a simple and efficient way to sample distinct bands of the pulse streams' spectrum. However, a drawback of this system is that it can only obtain a few constraint bands from the aliased spectrum, which reduces the utility of the signal spectrum and would affect the recovery performance in the presence of noise.

In this paper, we build on previous work in [22] and propose a more efficient way to obtain arbitrary frequency bands from the aliased spectrum, which improves the utility of the signal spectrum as well as the recovery performance in the presence of noise. Specifically, we propose a simplified multi-channel FRI sampling system for pulse streams to obtain the real parts of arbitrary bands of Fourier coefficients. This is achieved through modulating the input signal in each channel with a properly chosen cosine signal and then filtering with a LPF, followed by sampling at twice its cut-off frequency. The sampling structure is very simple, but the modulating process will lead to the signal spectrum aliasing and unavailable. Note that the zero-frequency component of the aliased spectrum is equal to the real part of the modulation-frequency component of the input signal spectrum. We propose a spectrum de-aliasing algorithm to calculate the real parts of the Fourier coefficients one by one from two staggered and aliased spectrums, which can be obtained from each two channels with close modulation frequencies. We next present a sparsity-based recovery algorithm to recover the time delays and amplitudes of the pulse streams by using these real parts of the Fourier coefficients. Finally, simulation results demonstrate the effectiveness and robustness of our system.

The remainder of the paper is organized as follows: Section III establishes the signal model of pulse streams and then proposes a FRI-based multi-channel sampling framework to obtain the real parts of distinct bands of Fourier coefficients. In Section IV, a sparsity-based recovery algorithm is proposed to estimate the time delays and amplitudes of pulse streams, by using the obtained real parts of the Fourier coefficients. Finally, Section V shows the results of MATLAB simulations and in Section VI we conclude with a brief summary.

II. NOMENCLATURE

The following notations are used throughout the paper.

L	Number of pulses
T	Observation time
ρ	The rate of innovation, $\rho = 2L/T$
f_s	Sampling rate
T_s	Sampling period, $T_s = 1/f_s$
ω_{cut}	Cutoff frequency of LPF
$\Delta\omega$	Frequency interval of the obtained real parts of the Fourier Coefficients
M	Quantizing number of bins for frequency period $[0, \omega_{cut})$ with step $\Delta\omega$, $M = \lfloor \frac{\omega_{cut}}{\Delta\omega} \rfloor$
P	Number of channels of the muti-channel sampling system
K	Total number of the obtained real parts of the Fourier Coefficients
N	Quantizing number of bins for time period $[0, T)$
δ	Quantizing step for time period $[0, T)$, $\delta = T/N$

III. OBTAIN REAL PARTS OF THE FOURIER COEFFICIENTS FROM THE ALIASED SPECTRUM

A. PROBLEM FORMULATION

In this work, our interest focuses on the sampling and recovering of signals consisting of a stream of short pulses, where the pulse shape is known. Such signals are typical FRI signals, and can be modeled as:

$$x(t) = \sum_{l=1}^{L} a_l h(t - t_l), a_l \in C, t_l \in [0, T), \tag{1}$$

where $h(t)$ is the known pulse shape with a short duration in time domain. Obviously, the only unknown parameters are time delays and amplitudes $\{a_l, t_l\}_{l=1}^{L}$. Thus, the pulse streams are essentially a delayed and scaled version of the known pulses, which can be thought of as a parametric signal.

Since $x(t)$ has $2L$ degrees of freedom within any length-T time interval, Dragotti *et al.* [15] shows that at least $2L$ samples (Fourier coefficients) per time T are required in order to recover the signal $x(t)$. That is, $x(t)$ can be sampled uniformly at the rate $f_s = \rho$ using an appropriate sampling kernel and then be perfectly reconstructed. If L/T is sufficiently small with respect to $h(t)$'s bandwidth, this implies a significant reduction in sampling rate.

Calculated with respect to a time period $[0, T)$, the continuous-time Fourier transform (CTFT) of $x(t)$ can be written as:

$$\begin{aligned} X(\omega) &= \int_{-\infty}^{\infty} [\sum_{l=1}^{L} a_l h(t - t_l)] e^{-j\omega t} dt \\ &= \sum_{l=1}^{L} a_l \int_{-\infty}^{\infty} h(t - t_l) e^{-j\omega t} dt \\ &= H(\omega) \sum_{l=1}^{L} a_l e^{-j\omega t_l}, \end{aligned} \tag{2}$$

where $H(\omega)$ is the CTFT of the known pulse $h(t)$. If we substitute $\omega = k\omega_0$, where k is an integer, Eq. (2) can be rewritten as:

$$X(k\omega_0) = H(k\omega_0) \sum_{l=1}^{L} a_l e^{-jk\omega_0 t_l}. \tag{3}$$

Because the transmit pulse $h(t)$ and its Fourier transform $H(\omega)$ are known, the parameters $\{a_l, t_l\}_{l=1}^{L}$ can be solved by acquiring a set of nonzero Fourier coefficients $X(k\omega_0)$, where $H(k\omega_0) \neq 0$. Many algorithms for solving (3) exist, among which are annihilating filter [2], matrix pencil [23], ESPRIT [24] and many others that can be found in [25].

B. FREQUENCY SELECTION AND SPECTRUM ALIASING PROBLEM

Acquiring a consecutive Fourier subset can be done using a LPF, followed by sampling at twice its cut-off frequency. The discrete Fourier transform (DFT) of the samples provides the desired Fourier coefficients. However, the recovery performance is enhanced when using a set of coefficients distributed over a larger part of the signal's spectrum. For the acquisition of an arbitrary set of Fourier coefficients, we have proposed a modulating and LPF based sampling scheme in [22]. In the proposed sampling setup depicted in Fig. 1, the original continuous-time signal $x(t)$ is modulated and then filtered before being (uniformly) sampled with sampling period T_s.

Firstly, the pulse streams $x(t)$ is modulated with a cosine signal $p(t)$, which can be written as:

$$p(t) = \cos(\omega_p t), \tag{4}$$

where ω_p is the frequency of the cosine signal and can be called modulation frequency. The CTFT of the modulation signal $p(t)$ is:

$$P(\omega) = \pi[\delta(\omega + \omega_p) + \delta(\omega - \omega_p)], \tag{5}$$

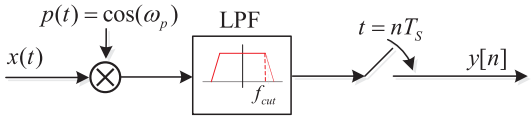

FIGURE 1. Sampling setup.Here, $x(t)$ is the pulse streams, $p(t)$ is the modulation signal, and T_S is the sampling period. The samples are $y[n]$.

where $P(\omega)$ is the CTFT of $p(t)$, $\delta(\omega)$ is the Dirac function. So the modulated signal can be described as $g(t) = x(t) \cdot p(t)$, and the CTFT of $y(t)$ is:

$$\begin{aligned} G(\omega) &= \frac{1}{2\pi} X(\omega) * P(\omega) \\ &= \frac{1}{2} X(\omega) * [\delta(\omega + \omega_p) + \delta(\omega - \omega_p)] \\ &= \frac{1}{2} [X(\omega + \omega_p) + X(\omega - \omega_p)], \end{aligned} \tag{6}$$

where $G(\omega)$ is the CTFT of the modulated signal $g(t)$, $X(\omega)$ is the CTFT of the input signal $x(t)$.

After the modulating process, the modulated signal $g(t)$ is filtered with a LPF, followed by sampling at twice its cut-off frequency with an analog-digital converter (ADC). Suppose that the signal $g(t)$ is filtered with an ideal LPF with cutoff frequency ω_{cut}, that is,

$$\begin{aligned} Y(\omega) &= rect(\frac{\omega}{2\omega_{cut}}) G(\omega) \\ &= \begin{cases} \frac{1}{2}[X(\omega + \omega_p) + X(\omega - \omega_p)], & |\omega| \leq \omega_{cut} \\ 0, & |\omega| > \omega_{cut}. \end{cases} \end{aligned} \tag{7}$$

Assume that $\omega_{\max}$ is the maximum frequency of $x(t)$, the modulating process can be divided into three cases:

Case 1, $\omega_p > \omega_{\max} + \omega_{cut}$. In this case, the modulated signal's Fourier spectrum is outside the low-pass frequency domain, as shown in Fig. 2(b). This will lead to a set of zero sampling values.

Case 2, $\omega_{\max} \leq \omega_p \leq \omega_{\max} + \omega_{cut}$. In this case, the modulated signal's Fourier spectrum is inside the low-pass frequency domain, as shown in Fig. 2(c). However, since $\omega_{cut} << \omega_{\max}$, modulating in this case will extremely reduce the Fourier spectrum utilization.

Case 3, $\omega_p < \omega_{\max}$. In this case, the modulating process would lead to spectrum aliasing problem, with the frequencies aliasing area $[-(\omega_{\max} - \omega_p), (\omega_{\max} - \omega_p)]$, as shown in Fig. 2(d). In [22] we have proposed a modulation frequency selection strategy to solve this spectrum aliasing problem, obtaining reconfigurable Fourier coefficients from the aliased spectrum. However, this system can only obtain a few constraint bands from the aliased spectrum, which reduces the utility of the signal spectrum and would affect the recovery performance in the presence of noise. In the the next subsection, we will remove this limitation and extend the sampling range to the entire Fourier spectrum

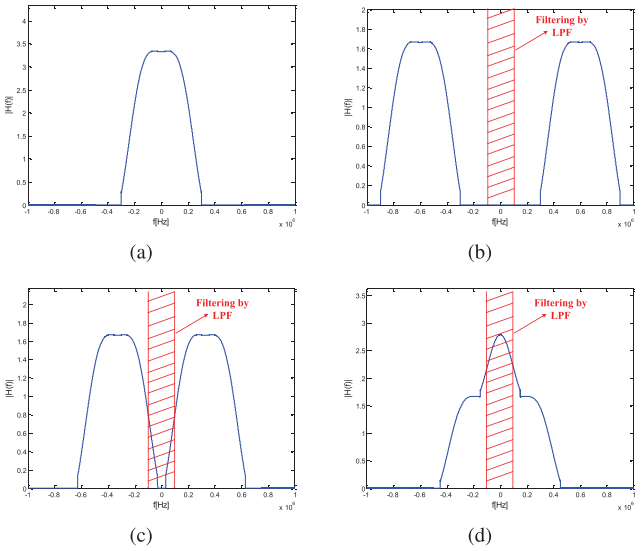

FIGURE 2. The modulating results: (a) Original signal spectrum; (b) *Case 1,* $\omega_p > \omega_{\max} + \omega_{cut}$; (c) *Case 2,* $\omega_{\max} < \omega_p \leq \omega_{\max} + \omega_{cut}$; and (d) *Case 3,* $\omega_p \leq \omega_{\max}$.

through obtaining the real parts of arbitrary bands of Fourier coefficients.

C. SPECTRUM DE-ALIASING

We use two modulation processes from different channels to solve the spectrum aliasing problem, which allows to extract the real parts of an arbitrary band of Fourier coefficients from the aliased spectrum.

Theorem 1: Consider pulse streams $x(t) = \sum_{l=1}^{L} a_l h(t - t_l)$, *with maximum frequency* $\omega_{\max}$. *The signal* $x(t)$ *is splited into two channels and modulated with cosine signals* $p_1(t) = \cos(\omega_1 t)$ *and* $p_2(t) = \cos((\omega_1 + \Delta\omega)t)$, *respectively. The modulated signal in each channel is then filtered with a LPF with cutoff frequency* ω_{cut}. *Assume that* $0 < \Delta\omega < \omega_{cut}$ *and* $0 < \omega_1 < \omega_{\max} - \Delta\omega$. $M = \lfloor \frac{\omega_{cut}}{\Delta\omega} \rfloor$, *and the CTFT of the filtered signals are denoted as* $Y_1(\omega)$ *and* $Y_2(\omega)$. *Then* $2M + 2$ *real parts of the Fourier coefficients of* $x(t)$ *can be extracted from these two aliased spectrums* $Y_1(\omega)$ *and* $Y_2(\omega)$. *Actually, we can obtain a set as:* $U = \{X_R(\omega_1 + b\Delta\omega) | b = -M, 1 - M, \cdots, M + 1\}$, *where* $X_R(\cdot)$ *denotes the real part of the Fourier coefficient* $X(\cdot)$.

Proof: Assuming that two modulation signals are $p_1(t) = \cos(\omega_1 t)$ and $p_2(t) = \cos((\omega_1 + \Delta\omega)t)$, where $0 < \Delta\omega < \omega_{cut}$, $0 < \omega_1 < \omega_{\max} - \Delta\omega$. It can be shown from Eq.(7) that these two aliased spectrums can be described as:

$$\begin{cases} Y_1(\omega) = \frac{1}{2}[X(\omega + \omega_1) + X(\omega - \omega_1)] \\ Y_2(\omega) = \frac{1}{2}[X(\omega + \omega_1 + \Delta\omega) + X(\omega - \omega_1 - \Delta\omega)], \end{cases} \tag{8}$$

where $|\omega| < \omega_{cut}$.

We begin by finding the relationship between $X(\omega)$ and $X(-\omega)$. Combining with the famous Euler's formula $e^{-j\omega} = \cos\omega - j\sin\omega$, the CTFT of the pulse streams $x(t)$ can be calculated as:

$$\begin{aligned} X(\omega) &= \int_{-\infty}^{\infty} x(t) e^{-j\omega t} dt \\ &= \int_{-\infty}^{\infty} x(t)[\cos(\omega t) - j\sin(\omega t)]dt \\ &= \int_{-\infty}^{\infty} x(t)\cos(\omega t)dt - j\int_{-\infty}^{\infty} x(t)\sin(\omega t)dt. \end{aligned} \tag{9}$$

Let $X^*(\omega)$ denote the complex conjugate of $X(\omega)$, we have:

$$\begin{aligned} X^*(\omega) &= \int_{-\infty}^{\infty} x(t)\cos(\omega t)dt + j\int_{-\infty}^{\infty} x(t)\sin(\omega t)dt \\ &= X(-\omega). \end{aligned} \tag{10}$$

Making use of this property, *i.e.,* $X^*(\omega) = X(-\omega)$, Eq.(8) can be rewritten as:

$$\begin{cases} Y_1(\omega) = \frac{1}{2}[X(\omega_1 + \omega) + X^*(\omega_1 - \omega)] \\ Y_2(\omega) = \frac{1}{2}[X(\omega_1 + \Delta\omega + \omega) + X^*(\omega_1 + \Delta\omega - \omega)], \end{cases} \tag{11}$$

where $|\omega| < \omega_{cut}$. Next we will discuss the steps required to recover $X(\omega)$ from the above formula. In practice, we would like to obtain a set of real parts of the Fourier coefficients as $\{X_R(\omega_1), X_R(\omega_1 \pm \Delta\omega), X_R(\omega_1 \pm 2\Delta\omega), \cdots\}$, where $X_R(\omega)$ denotes the real part of $X(\omega)$.

Firstly, calculate the initial values. Let $\omega = 0$, Eq.(11) can be rewritten as:

$$\begin{cases} Y_1(0) = \frac{1}{2}[X(\omega_1) + X^*(\omega_1)] = X_R(\omega_1) \\ Y_2(0) = \frac{1}{2}[X(\omega_1 + \Delta\omega) + X^*(\omega_1 + \Delta\omega)] \\ = X_R(\omega_1 + \Delta\omega). \end{cases} \tag{12}$$

In this way, we can obtain two real parts of the Fourier coefficients from the zero-frequency component of the aliased spectrum, *i.e.,* $X_R(\omega_1) = Y_1(0)$ and $X_R(\omega_1 + \Delta\omega) = Y_2(0)$.

Secondly, deduce the iterative formula. If $M = \lfloor \frac{\omega_{cut}}{\Delta\omega} \rfloor \geq 1$, we can obtain more real parts of the Fourier coefficients from the aliased spectrum. Let $\omega = m\Delta\omega$, where $m = 1, 2, \cdots, M$. From Eq. (11) we can calculate the CTFT of the first filtered signal:

$$\begin{aligned} Y_1(m\Delta\omega) &= \frac{1}{2}[X(\omega_1 + m\Delta\omega) + X^*(\omega_1 - m\Delta\omega)] \\ \Rightarrow X^*(\omega_1 - m\Delta\omega) &= 2Y_1(m\Delta\omega) - X(\omega_1 + m\Delta\omega) \\ \Rightarrow X_R(\omega_1 - m\Delta\omega) &= 2Y_{1R}(m\Delta\omega) - X_R(\omega_1 + m\Delta\omega), \end{aligned} \tag{13}$$

where $Y_{1R}(\omega)$ denote the real part of $Y_1(\omega)$. Similarly, from Eq.(11) we can also calculate the CTFT of the second filtered signal:

$$\begin{aligned} Y_2(m\Delta\omega) = \frac{1}{2}[&X(\omega_1 + (m+1)\Delta\omega) \\ &+ X^*(\omega_1 - (m-1)\Delta\omega)] \\ \Rightarrow X_R(\omega_1 + (m+1)\Delta\omega) &= 2Y_{2R}(m\Delta\omega) \\ &- X_R(\omega_1 - (m-1)\Delta\omega) \end{aligned} \tag{14}$$

where $Y_{2R}(\omega)$ denotes the real part of $Y_2(\omega)$.

In conclusion, we can easily deduce the iterative formula from Eq.(13) and Eq.(14), combining with the initial values

$X_R(\omega_1)$ and $X_R(\omega_1+\Delta\omega)$ in Eq.(12). The iterative formula of the spectrum de-aliasing process can be described as:

$$\begin{cases} X_R(\omega_1) = Y_1(0) \\ X_R(\omega_1+\Delta\omega) = Y_2(0) \\ X_R(\omega_1 - m\Delta\omega) = 2Y_{1R}(m\Delta\omega) - X_R(\omega_1 + m\Delta\omega) \\ X_R(\omega_1+(m+1)\Delta\omega) = X_R(\omega_1+(m-1)\Delta\omega) \\ -2Y_{1R}((m-1)\Delta\omega) + 2Y_{2R}(m\Delta\omega), \end{cases} \quad (15)$$

where $m = 1, 2, \cdots, M$ and $M = \left\lfloor \frac{\omega_{cut}}{\Delta\omega} \right\rfloor \geq 1$. Thus, by using the above iterative formula, we can get $2M+2$ real parts of the Fourier coefficients, which can be described as:

$$U = \{X_R(\omega_1 + b\Delta\omega) | b = -M, 1-M, \cdots, M+1\} \quad (16)$$

where U is a set of real parts of the Fourier coefficients of the pulse streams $x(t)$. ■

The spectrum de-aliasing algorithm is summarized in Algorithm 1. We can easily obtain a set of real parts of the Fourier coefficients from each two sampling channels, by using Algorithm 1. In the the next subsection, we will propose a multi-channel sampling structure, aiming to obtain the real parts of arbitrary and discrete bands of Fourier coefficients.

Algorithm 1 Spectrum De-Aliasing Algorithm

Require: Modulation frequency ω_1 and $\Delta\omega$; The corresponding aliased spectrum $Y_1(\omega)$ and $Y_2(\omega)$; Cutoff frequency of LPF ω_{cut}.

Ensure: A set of real parts of the Fourier coefficients U.

1: $X_R(\omega_1) = Y_1(0)$. (Calculate the initial value).
2: $X_R(\omega_1+\Delta\omega) = Y_2(0)$. (Calculate the initial value).
3: $M = \left\lfloor \frac{\omega_{cut}}{\Delta\omega} \right\rfloor$.
4: **if** $M = 0$ **then**
5: $U = \{X_R(\omega_1), X_R(\omega_1+\Delta\omega)\}$. (Obtain 2 real parts of the Fourier coefficients).
6: **else**
7: **for** $m = 1$ to M **do**
8: $X_R(\omega_1 - m\Delta\omega) = 2Y_{1R}(m\Delta\omega) - X_R(\omega_1 + m\Delta\omega)$.
9: $X_R(\omega_1+(m+1)\Delta\omega) = X_R(\omega_1+(m-1)\Delta\omega) - 2Y_{1R}((m-1)\Delta\omega) + 2Y_{2R}(m\Delta\omega)$.
10: **end for**
11: $U = \{X_R(\omega_1 + b\Delta\omega) | b = -M, 1-M, \cdots, M+1\}$. (Obtain $2M+2$ real parts of the Fourier coefficients).
12: **end if**

D. MULTI-CHANNEL SAMPLING STRUCTURE

In [26], it was suggested to use a non-consecutive set of Fourier coefficients selected in a distributed manner, as many detection systems (*e.g.,* ultrasound in [26] and radar in [21]) benefit from wide frequency aperture. It is also shown in [21] that a distributed selection of the signal spectrum results in better recovery and noise robustness than consecutive coefficients.

Here we present a simplified multi-channel sampling system to obtain the real parts of the Fourier coefficients in a manner that is both practical and efficient. This approach makes use of several parallel channels in which the real parts of distinct bands of the signal spectrum are obtained, as illustrated in Fig. 3.

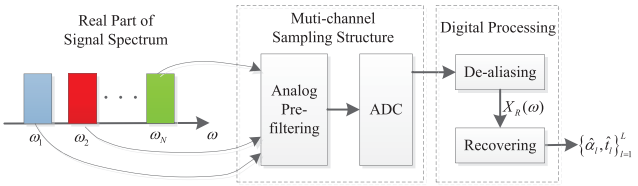

FIGURE 3. Multi-channel sampling of pulse streams.

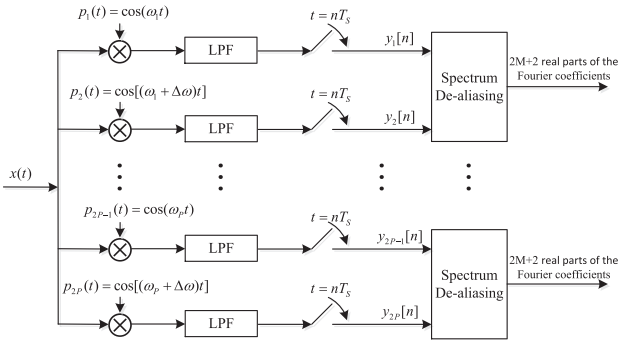

FIGURE 4. Multi-channel sampling structure. Here, each two sampling channels can obtain $2M+2$ ($M = \left\lfloor \frac{\omega_{cut}}{\Delta\omega} \right\rfloor$) real parts of the Fourier coefficients.

The proposed multi-channel sampling structure is shown in Fig. 4. It mainly consists of a multiplier, a LPF and a low rate ADC in each channel. The DFT of the samples provide the signal spectrum. The real parts of a band of Fourier coefficients can be obtained from each two sampling channels, in which the signal $x(t)$ is modulated with cosine signals $p_{2i-1} = \cos(\omega_i t)$ and $p_{2i} = \cos((\omega_i+\Delta\omega)t)$ $(i = 1, 2, \cdots, P)$, respectively. The modulation frequencies should satisfy $0 < \Delta\omega < \omega_{cut}$ and $0 < \omega_i < \omega_{\max} - \Delta\omega$, where $\omega_{\max}$ is the maximum frequency of the input pulse streams $x(t)$, and ω_{cut} is the cutoff frequency of the LPF. In this way, we can obtain $2M+2$ ($M = \left\lfloor \frac{\omega_{cut}}{\Delta\omega} \right\rfloor$) real parts of the Fourier coefficients from channel $2i-1$ and channel $2i$, by using Algorithm 1. That is, the obtained real parts of the Fourier coefficients are $U_i = \{X_R(\omega_i + b\Delta\omega) | b = -M, 1-M, \cdots, M+1\}$. For the convenience of calculation, we set $\omega_i = m_i\Delta\omega$, where m_i is a positive integer. Then the obtained real parts of the Fourier coefficients can be expressed as:

$$U_i = \{X_R((m_i+b)\Delta\omega) | m_i = \frac{\omega_i}{\Delta\omega}; \\ b = -M, 1-M, \cdots, M+1\}. \quad (17)$$

We use $2P$ sampling channels to obtain the real parts of P bands of Fourier coefficients. In order to separate the bands from each other, the modulation frequencies should satisfy:

$$|\omega_i - \omega_j| \geq 2\omega_{cut} + \Delta\omega, \quad \forall i \neq j, \quad (18)$$

where $i, j = 1, 2, \cdots, P$. Then, we can obtain $(2M+2)P$ real parts of the Fourier coefficients from all $2P$ channels:

$$U = \{U_1, U_2, \cdots, U_P\}, \tag{19}$$

where U is usually called as the measurements. Finally, by using a sparsity-based recovery algorithm introduced in Section IV, the time delay and amplitude parameters of the pulse streams $x(t)$ can be estimated with $K = (2M+2)P \geq cL\log(N/L) \ll N$ real parts of the Fourier coefficients, with c a small constant and N the quantizing number of bins. So the proposed multi-channel sampling structure can sample the pulse streams $x(t)$ with perfect reconstruction at a sub-Nyquist rate.

To illustrate the proposed muti-channel sampling system more clearly, we show how to set the system parameters as follows. Firstly, the signal $x(t)$ is formed by L pulses in the time period $[0, T)$ and has the highest frequency $\omega_{\max}$. Secondly, the number of channels, the cutoff frequency of LPF and the frequency interval of the obtained real parts of the Fourier coefficients are set as $2P$, ω_{cut} and $\Delta\omega$, respectively, and should satisfy $0 < \Delta\omega < \omega_{cut} < \omega_{\max}$. Thirdly, the modulation frequencies are set as $\omega_i = m_i\Delta\omega$, where $i = 1, 2, \cdots, P$ and m_i is a positive integer, and should satisfy Eq. (18). Denote $M = \lfloor \frac{\omega_{cut}}{\Delta\omega} \rfloor$, then $K = (2M+2)P$ real parts of the Fourier coefficients can be obtained from the proposed $2P$-channel sampling system. Finally, the quantizing number of bins for time period $[0, T)$ is set as N. Furthermore, in order to recover the $2L$ parameters $\{a_l, t_l\}_{l=1}^{L}$ of $x(t)$, the system parameters P, ω_{cut} and $\Delta\omega$ should satisfy $K = (2\lfloor \frac{\omega_{cut}}{\Delta\omega} \rfloor + 2)P \geq cL\log(N/L)$, with c a small constant.

IV. RECOVERY ALGORITHM

A. RECOVERY PROBLEM

Having gone through the sampling stage, we will now discuss the recovery process by using these real parts of the Fourier coefficients. Assume that we have obtained $K = (2M+2)P$ real parts of the Fourier coefficients from the proposed sampling system. The measurements $U = \{X_R(k\Delta\omega)\}_{k\in\kappa}$, where $\kappa = \{m_i + b | m_i = \frac{\omega_i}{\Delta\omega}; i = 1, 2, \cdots, P; b = -M, 1-M, \cdots, M+1\}$. Since the Fourier coefficients of the known pulse $H(k\Delta\omega)$ is a complex number, it can be expressed as:

$$H(k\Delta\omega) = c_k e^{j\varphi_k}, \tag{20}$$

where c_k is the modulus and φ_k is the phase. Recall $e^{-jk\omega_0 t_l} = \cos k\omega_0 t_l - j\sin k\omega_0 t_l$ and let $\omega_0 = \Delta\omega$, (3) can be rewritten as:

$$\begin{aligned} X(k\Delta\omega) &= H(k\Delta\omega)\sum_{l=1}^{L} a_l e^{-jk\Delta\omega t_l} \\ &= \sum_{l=1}^{L} a_l c_k e^{-j(k\Delta\omega t_l - \varphi_k)} \\ &= \sum_{l=1}^{L} a_l c_k [\cos(k\Delta\omega t_l - \varphi_k) - j\sin(k\Delta\omega t_l - \varphi_k)]. \end{aligned} \tag{21}$$

Extracting the real part from (21):

$$X_R(k\Delta\omega) = \sum_{l=1}^{L} a_l c_k \cos(k\Delta\omega t_l - \varphi_k). \tag{22}$$

Obviously, there are only $2L$ unknown parameters $\{a_l, t_l\}_{l=1}^{L}$ in (22). So it can be solved given a set of nonzero real parts of the Fourier coefficients $X_R(k\Delta\omega)$. In the next subsection, we will show how to recover the parameters $\{a_l, t_l\}_{l=1}^{L}$ from the measurements $U = \{X_R(k\Delta\omega)\}_{k\in\kappa}$.

B. SPARSITY-BASED RECOVERY ALGORITHM

Theorem 2: Consider pulse streams $x(t) = \sum_{l=1}^{L} a_l h(t - t_l)$, $t \in [0, T)$, where the pulse shape $h(t)$ and number of pulses L are known. If the analog time $t \in [0, T)$ is quantified into N uniform bins, then the unknown time delay and amplitude parameters $\{a_l, t_l\}_{l=1}^{L}$ can be recovered through $K \geq cL\log(N/L) \ll N$ real parts of the Fourier coefficients, with c a small constant.

Proof: We begin by quantizing the analog time axis with a resolution step of δ. Thus, the analog time t can be approximated to $t = n\delta$, with $n = 0, 1, \ldots, N-1$ and $N = T/\delta$. The unknown time delay parameters can be expressed as $t_l \approx n_l\delta$, where $n_l \in \{0, 1\cdots, N-1\}$ is the discrete numeric value of time delays t_l. In this way, equation (22) can be approximated as:

$$X_R(k\Delta\omega) \approx \sum_{l=1}^{L} a_l c_k \cos(k\Delta\omega n_l\delta - \varphi_k), \tag{23}$$

where $k = \kappa_1, \kappa_2, \cdots, \kappa_K$, with κ_i $(i = 1, 2, \cdots, K)$ the fundamental element of the set κ. It can be written in matrix form as follows:

$$\begin{bmatrix} u_{\kappa_1} \\ u_{\kappa_2} \\ \vdots \\ u_{\kappa_K} \end{bmatrix} = \begin{bmatrix} d_{\kappa_1,n_1} & \cdots & d_{\kappa_1,n_L} \\ d_{\kappa_2,n_1} & \cdots & d_{\kappa_2,n_L} \\ \vdots & \ddots & \vdots \\ d_{\kappa_K,n_1} & \cdots & d_{\kappa_K,n_L} \end{bmatrix} \cdot \begin{bmatrix} a_1 \\ a_2 \\ \vdots \\ a_L \end{bmatrix}, \tag{24}$$

where $u_{\kappa_i} = X_R(\kappa_i\Delta\omega)$ and $d_{\kappa_i,n_l} = c_{\kappa_i}\cos(\kappa_i\Delta\omega n_l\delta - \varphi_{\kappa_i})$, with κ_i $(i = 1, 2, \cdots, K)$ the fundamental element of the set κ.

Considering that the time domain of the pulse streams $x(t)$ is limited to $t_l \in [0, T)$, a complete set of the analog time can be obtained as $\eta = \{0, \delta, 2\delta, \cdots, (N-1)\delta\}$ with $N = T/\delta$, in the condition of ignoring quantization error. Thus the time delays parameters set is $\gamma = \{n_0\delta, n_1\delta, \cdots, n_{L-1}\delta\}$, which constitute a smaller subset of the set η, that is $\gamma \subset \eta$ with $L \ll N$. Thus, if we replace the time delay parameters set γ with its complete set η, Eq.(24) can be rewritten as a sparsity matrix:

$$\begin{bmatrix} u_{\kappa_1} \\ u_{\kappa_2} \\ \vdots \\ u_{\kappa_K} \end{bmatrix} = \begin{bmatrix} d_{\kappa_1,0} & \cdots & d_{\kappa_1,N-1} \\ d_{\kappa_2,0} & \cdots & d_{\kappa_2,N-1} \\ \vdots & \ddots & \vdots \\ d_{\kappa_K,0} & \cdots & d_{\kappa_K,N-1} \end{bmatrix} \cdot \begin{bmatrix} s_0 \\ s_1 \\ \vdots \\ s_{N-1} \end{bmatrix}, \tag{25}$$

where $[s_0, s_1, \cdots, s_{N-1}]^T$ is a $N \times 1$ vector, formed by L amplitude parameters $\{a_l\}_{l=1}^{L}$ and $N - L$ zero values.

That is, $a_l = s_{n_l}$, where $l = 1, 2, \cdots, L$ and $n_l \in \{0, 1, \cdots, N-1\}$. Our goal is to find the nonzero entries of the vector $[s_0, s_1, \cdots, s_{N-1}]^T$ from the measurement values. For simplicity, Eq.(25) may be written as:

$$u = \Phi s, \tag{26}$$

where u is a $K \times 1$ vector formed by K nonzero measurements u_{κ_i}, with $i = 1, 2, \cdots, K$; $\Phi = [\phi_{\kappa_1}; \phi_{\kappa_2}; \cdots; \phi_{\kappa_K}]$ is a $K \times N$ matrix formed by the vector $\phi_{\kappa_i} = c_{\kappa_i}[\cos(\varphi_{\kappa_i}), \cos(\kappa_i \Delta\omega\delta - \varphi_{\kappa_i}), \cdots, \cos(\kappa_i \Delta\omega(N-1)\delta - \varphi_{\kappa_i})]$, with κ_i $(i = 1, 2, \cdots, K)$ the fundamental element of the set κ; $s \in R^{N\times 1}$ is an L-sparse vector with nonzero entries at indices $\{n_l\}_{l=0}^{L-1}$, and the corresponding nonzero element values are $\{a_l\}_{l=0}^{L-1}$.

The most direct way to solve Eq.(26) is by solving a L0 norm optimization problem described as:

$$\begin{cases} \hat{s} = \arg\min ||s||_0 \\ s.t. u = \Phi s, \end{cases} \tag{27}$$

where the L0 norm $||s||_0$ means the number of non-zero coefficients in vector s. Solving Eq.(27) is an NP-hard problem. The solution can be obtained, for example, by using the well-known orthogonal matching pursuit (OMP) algorithm [27]–[30]. The algorithm iteratively finds the nonzero entries of s by seeking the maximal correlations between u and the columns of Φ, while maintaining an orthogonalization step at the end of each iteration. It is showed in [27] and [28] that the L-sparse signal s of length N can be recovered from only $K \geq cL\log(N/L) \ll N$ measurements, with c a small constant.

Once the L-sparse signal s is solved, the position of the nonzero elements $n_l (l = 1, 2, \cdots, L)$ can be known. Then the time delay parameters can be directly calculated as $\hat{t}_l = \hat{n}_l \delta$, and the amplitude parameters are estimated via $\hat{a}_l = s[\hat{n}_l]$. As the pulse streams is essentially a delayed and scaled version of the pulse $h(t)$, the original signal $x(t)$ can be perfectly recovered if we know the pulse shape. That is,

$$\hat{x}(t) = \sum_{l=1}^{L} \hat{a}_l h(t - \hat{t}_l), \quad t \in [0, T), \tag{28}$$

where T is the observation time. ■

A pseudo-code of the proposed sparsity-based recovery algorithm is given in Algorithm 2. Obviously, Algorithm 2 requires that the time delays $\{t_l\}_{l=1}^{L}$ are all on the grids, that is, the quantization error should be ignored. However, such situation is not common in practice. We will analyze the effect of the quantization error in the next subsection.

C. EFFECT OF THE QUANTIZATION ERROR

Assume that the unknown time delay parameters can be expressed as $t_l = n_l\delta + \sigma_l$, where $n_l \in \{0, 1 \cdots, N-1\}$ is the discrete numeric value of time delays t_l and $\sigma_l \in [0, \delta)$ is the quantization error. In this way, equation (22) may be rewritten as:

$$\begin{aligned} X_R(k\Delta\omega) &= \sum_{l=1}^{L} a_l c_k \cos(k\Delta\omega n_l\delta + k\Delta\omega\sigma_l - \varphi_k) \\ &= \sum_{l=1}^{L} a_l c_k [\cos(k\Delta\omega n_l\delta - \varphi_k)\cos(k\Delta\omega\sigma_l) \\ &\quad - \sin(k\Delta\omega n_l\delta - \varphi_k)\sin(k\Delta\omega\sigma_l)]. \end{aligned} \tag{29}$$

Because the DFT of the samples provide the Fourier coefficients, we set $\Delta\omega = \frac{2\pi}{T}$ for convenience. Since $0 \leq k\sigma_l < K\delta \ll T$, we have $\sin(k\Delta\omega\sigma_l) \to 0$ and $\cos(k\Delta\omega\sigma_l) \to 1$. If we substitute $a_l^* = a_l \cos(k\Delta\omega\sigma_l)$, (29) can be transformed into:

$$X_R(k\Delta\omega) \approx \sum_{l=1}^{L} a_l^* c_k \cos(k\Delta\omega n_l\delta - \varphi_k). \tag{30}$$

Obviously, (23) is an approximate version of (30). So the quantization error would lead to an attenuation of the estimated amplitude parameters, *i.e.*, $\hat{a}_l = a_l^* = \mu_l a_l$ with $\mu_l = \cos(k\Delta\omega\sigma_l) \to 1$.

The time delays can be estimated as $\hat{t}_l = \hat{n}_l\delta$, with $l = 1, 2, \cdots, L$. It is showed in [27] that $\hat{n}_l \approx n_l$ when the number of measurements $K \geq cL\log(N/L)$, with c a small constant. So we have $\hat{t}_l \approx n_l\delta = t_l - \sigma_l$. The quantization error would also lead to a deviation of the estimated time delay parameters. Note that $0 \leq \sigma_l < \delta = \frac{T}{N}$, we have $t_l - \frac{T}{N} < \hat{t}_l \leq t_l$. So the reconstruction error of time delays can be minimized through increasing the number of bins N.

Algorithm 2 Sparsity-Based Recovery Algorithm

Require: Pulse spectrum $H(\omega)$; Number of pulses L; Observation time T; Quantizing number of bins N; K measurements $U = \{X_R(k\Delta\omega)\}_{k\in\kappa}$, with $K \geq cL\log(N/L) \ll N$.

Ensure: Estimated time delays $\{\hat{t}_l\}_{l=1}^{L}$; Corresponding estimated amplitudes $\{\hat{a}_l\}_{l=1}^{L}$.

1: $\delta = T/N$. (Quantify the the analog time axis).
2: **for** $i = 1$ to K **do**
3: $k = \kappa_i$.
4: $c_k = abs(H(k\Delta\omega))$. (The modulus of $H(k\Delta\omega)$).
5: $\varphi_k = angle(H(k\Delta\omega))$. (The phase of $H(k\Delta\omega)$).
6: $\phi_k = c_k[\cos(\varphi_k), \cos(k\Delta\omega\delta - \varphi_k), \cdots, \cos(k\Delta\omega(N-1)\delta - \varphi_k)]$.
7: **end for**
8: $\Phi = [\phi_1; \phi_2; \cdots; \phi_K]$. (Calculate the measurement matrix).
9: $u = \Phi s$. (Solve the sparse solution $\hat{s}$ with the OMP algorithm in [27] and [28]).
10: $\{\hat{n}_l\}_{l=1}^{L} = \text{find}(\hat{s} \neq 0)$. (Find the positions of the nonzero elements).
11: $\hat{t}_l = \hat{n}_l\Delta$. (Estimate the time delays).
12: $\hat{a}_l = s[\hat{n}_l]$. (Estimate the amplitudes).

Denote the reconstruction error of the time delays t_l as:

$$error_l = \frac{|\hat{t}_l - t_l|}{|t_l|}. \tag{31}$$

To guarantee the reconstruction error $error_l \leq E$, with $E \in (0, 1)$, the number of quantization bins should satisfy $N \geq \frac{T}{E \cdot \min\{t_1, t_2, \cdots, t_L\}}$.

D. NOISE AND MODEL MISMATCH

Our algorithm can perfectly reconstruct pulse streams with known shapes in noiseless settings. It is then natural to wonder how it would perform when noise is present or when there is model mismatch. Consider the signal $x(t)$ with additive noise $w(t)$, which can be written as:

$$\bar{x}(t) = x(t) + w(t). \tag{32}$$

Then the noise measurements in Eq. (22) can be expressed as:

$$\begin{aligned} \bar{X}_R(k\Delta\omega) &= X_R(k\Delta\omega) + W_R(k\Delta\omega) \\ &= \sum_{l=1}^{L} a_l c_k \cos(k\Delta\omega t_l - \varphi_k) + w_k, \end{aligned} \tag{33}$$

where $w_k = W_R(k\Delta\omega)$, with $W_R(\omega)$ the the real part of the Fourier coefficient of $w(t)$.

Then we consider the model mismatch problem. In many practical cases of interest, the pulse shape may be distorted due to physical properties of propagation and transmission. For example, the signal would experience fading and shadowing effect during the transmission in wireless communication. Assume that the Fourier coefficients of the distorted version of the pulse shape $h(t)$ can be expressed as:

$$\begin{aligned} \tilde{H}(k\Delta\omega) &= H(k\Delta\omega) + r_k e^{j\theta_k} \\ &= c_k e^{j\varphi_k} + r_k e^{j\theta_k} \end{aligned} \tag{34}$$

where $r_k e^{j\theta_k}$ is the offset from $H(k\Delta\omega)$ to $\tilde{H}(k\Delta\omega)$, with r_k the modulus and θ_k the phase. Then the distorted measurements can be calculated as:

$$\begin{aligned} &\tilde{X}(k\Delta\omega) \\ &= \tilde{H}(k\Delta\omega) \sum_{l=1}^{L} a_l e^{-jk\Delta\omega t_l} \\ &= \sum_{l=1}^{L} a_l c_k e^{-j(k\Delta\omega t_l - \varphi_k)} + \sum_{l=1}^{L} a_l r_k e^{-j(k\Delta\omega t_l - \theta_k)} \\ &\Rightarrow \tilde{X}_R(k\Delta\omega) = \sum_{l=1}^{L} a_l c_k \cos(k\Delta\omega t_l - \varphi_k) + b_k, \end{aligned} \tag{35}$$

where $b_k = \sum_{l=1}^{L} a_l r_k \cos(k\Delta\omega t_l - \theta_k)$. So the distorted measurements $\tilde{X}_R(k\Delta\omega)$ have similar function model with the noise measurements $\bar{X}_R(k\Delta\omega)$ in Eq. (33).

In order to address the problems with noise and model mismatch and improve the robustness of our system, we can employ several strategies as follows. Firstly, to improve the temporal resolution and avoid the ambiguity of the time delay parameters [21], a wider frequency aperture can be obtained by appropriately selecting the modulation frequencies $\{\omega_i\}_{i=1}^{P}$. Secondly, to achieve more robust recovery of the CS formulation of (26), more measurements [31], [32] can be generated by selecting higher cutoff frequency of LPF, smaller frequency interval of the obtained real parts of the Fourier coefficients and more sampling channels. Thirdly, to improve the robustness and the estimation accuracy of the time delay parameters, a larger quantizing number of bins for time period $[0, T)$, *i.e.,* N, can be selected in accordance with the guideline in [20], [21], and [33]. Finally, to obtain a more robust solution of the L0 norm optimization problem (27) with the noisy measurements, the improved OMP algorithm [34] can be used.

V. SIMULATIONS

In this section we provide several experiments in which we examine various aspects of our method. The simulations are divided into 4 parts: 1)

1) Demonstration of the effectiveness for pulse streams with a large number of pulses overlapped in time domain;
2) Verification of the stability of the system with the number of pulses increasing;
3) Analysis of the effect of quantization error to the recovery method;
4) Evaluation of the performance in the presence of noise, and comparison to other techniques.

We examined our technique's success in recovering the pulse streams defined in (1): The basic pulse shape is *Sinc* function $h(t) = \text{sinc}(2Bt)$, with the maximum frequency $\omega_{\max} = B = 20e3(rad/s)$; Time delays are drawn uniformly, at random, within the intervals $[0, 1)sec$ and the amplitudes of the pulses varied randomly between $(0, 1]$. Throughout this section we consider the four-channel sampling structure, which can obtain the real parts of two bands of Fourier coefficients. The four modulation signals are:

$$\begin{cases} p_1(t) = \cos(\omega_1 t) \\ p_2(t) = \cos((\omega_1 + \Delta\omega)t) \\ p_3(t) = \cos(\omega_2 t) \\ p_4(t) = \cos((\omega_2 + \Delta\omega)t), \end{cases} \tag{36}$$

where $\omega_1 = 2\pi f_1$ and $\omega_2 = 2\pi f_2$, with f_1 and f_2 randomly selected in $\{1, 2, \cdots, 20\}\, kHz$; $\Delta\omega = 2\pi(rad/s)$. The cutoff frequency of LPF is $\omega_{cut} = 200\pi(rad/s)$. So we can obtain $K = (2M+2)\times 2 = 404$ real parts of the Fourier coefficients, where $M = \lfloor \frac{\omega_{cut}}{\Delta\omega} \rfloor = 100$.

In the recovering process, we quantify the analog time axis with the same step as $\delta = 0.001$ sec. To measure the recovery performance of the system, mean squared error (MSE) was considered as the evaluation index. For better comparison, the logarithm of MSE was considered:

$$MSE[dB] = 10\log_{10}\left(\frac{1}{L}\sum_{l=0}^{L-1}(t_l - \hat{t}_l)^2\right). \tag{37}$$

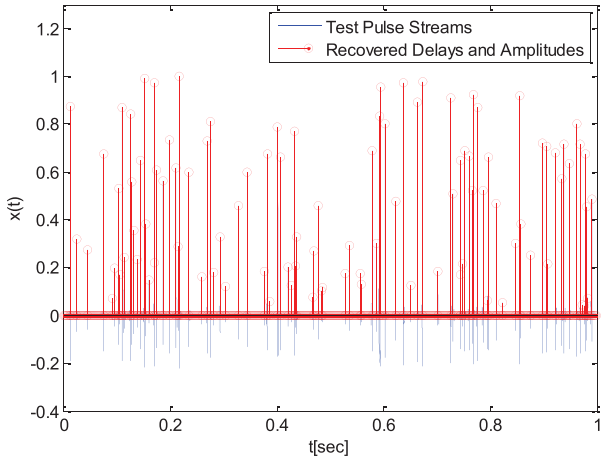

FIGURE 5. Performance for signal with 100 pulses.

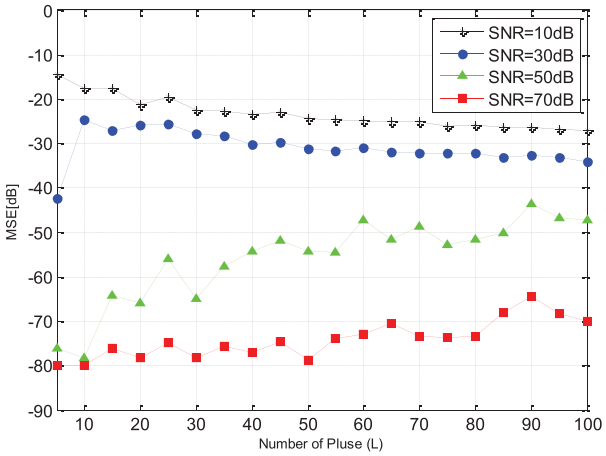

FIGURE 6. Simulation results with the number of pulses increasing.

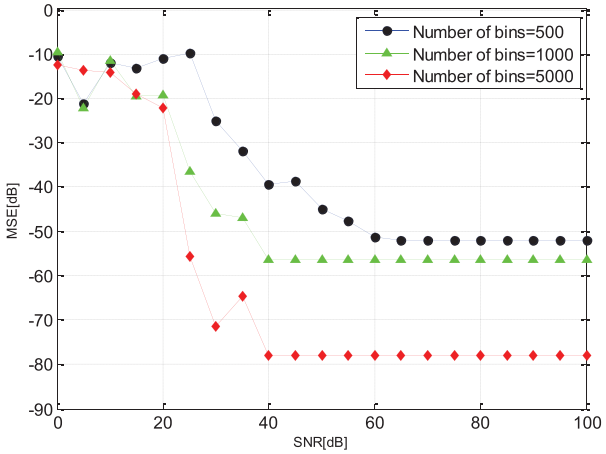

FIGURE 7. Simulation results under different quantization resolutions.

where L is the number of pulses, t_l is the true values and $\hat{t}_l$ is the estimated time delays. Because the error in the amplitudes is proportional to the error in the time instants, we only use the MSE in the time instants to measure the efficiency of the method.

Simulation 1: The first experiment step we introduce is examining the effectiveness of our method for pulse streams with high rate of innovation. Fig. 5 shows the performance of our system in condition that 100 noise free pulses were overlapped randomly in time domain. It can be seen that the time delays and amplitudes were recovered with high precision.

Simulation 2: Then we examined the the performance of our method for a large number of pulses corrupted by white Gaussian noise. The experimental tests were carried out 30 times, with the number of pulses increased from 1 to 100. The average recovery results under noise environment are illustrated in Fig. 6. The figure showed that the recovery curves all have very little up-and-down motion with the number of pulse increasing. It means that our method has little influence on the input signal's rate of innovation even in the presence of noise. We can also conclude that the recovery performance improved with the signal-to-noise ratio (SNR) level increasing.

Simulation 3: The next experiment is aim to measure the performance of the recovery method under different quantization accuracy. We examined the proposed method in recovering 10 Sinc pulses, after its corruption by noise. A typical reconstruction of the pulse streams is illustrated in Fig. 7. The results showed that the recovery accuracy improved with the number of bins (N) increasing, which means that dense quantizing could minimize the effect of the quantization error.

Simulation 4: Finally, we demonstrate the performance of our method in the presence of white Gaussian noise and compare to other Fourier spectrum based methods. In practice, we compare our results to those achieved by the LPF-based methods (annihilating filter [2] and state space method [35]) and the multi-channel method in [22], since these approaches all sample the Fourier spectrum. In this experiment we set the number of pulses $L = 8$ and the quantizing number of bins $N = 1000$. We consider the 4-channel FRI sampling system with OMP recovery algorithm in [22]. The modulation frequencies are $[1, 5, 7, 8]$ kHz and the cutoff frequency of LPF is $200\pi(rad/s)$. For better comparison, we quantify the analog time axis with the same step as 0.001 sec. Since we quantify the analog time axis with the same step and solve the CS formulation with the same OMP algorithm, the computational cost of the proposed method and the 4-channel (OMP) method is similarly the same. The MSE of the estimated time delays is depicted in Fig. 8, for all methods. Evidently, our approach outperforms the LPF based annihilating filter and state space method at lower SNR values. This corresponds to the fact that in noisy realizations the frequency aperture is critical. As the SNR increases, the frequency aperture plays a less significant role, and the total number of samples determines the reconstruction performance. Examining the results we also infer that our method yields better performance than the multi-channel method in [22], which can only obtain constraint band of the signal spectrum. But as the SNR improves

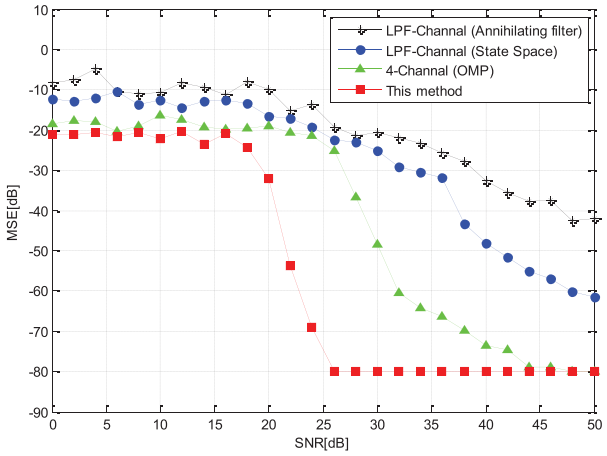

FIGURE 8. Comparison of different approaches.

the performance gap drops and finally coincides. For high enough SNR values, the quantization accuracy determines the recovery performance of the 4-channel (OMP) method and our method.

The LPF based methods can only extract a consecutive band and the 4-channel (OMP) method can extract 4 constraint bands of the signal spectrum. However, as discussed in [21], recovery performance is enhanced when using a set of coefficients distributed over a larger part of the signal's spectrum. So it is not surprising that our method has better recovery performance and noise robustness, since we provide a flexible selection of the signal spectrum.

VI. CONCLUSIONS

In this work, we propose a new FRI sampling scheme for pulse streams, which is based on sampling and recovering with the real parts of the Fourier coefficients. The proposed sampling structure mainly consists of a multiplier, a LPF and a low rate ADC in each channel, which is very simple and can be easily implemented in hardware. Combining with a spectrum de-aliasing algorithm, it can easily extract the real parts of distinct bands of Fourier coefficients from the aliased signal spectrum. We also propose a sparsity-based recovery algorithm to recover the pulse delays and amplitudes with these real parts of the Fourier coefficients. As we demonstrate by simulation, our method performs stably even many pulses are overlapped randomly in time domain, and exhibits better noise robustness than previous works.

REFERENCES

[1] M. Unser, "Sampling-50 years after Shannon," *Proc. IEEE*, vol. 88, no. 4, pp. 569–587, Apr. 2000.
[2] M. Vetterli, P. Marziliano, and T. Blu, "Sampling signals with finite rate of innovation," *IEEE Trans. Signal Process.*, vol. 50, no. 6, pp. 1417–1428, Jun. 2002.
[3] I. Maravic and M. Vetterli, "Sampling and reconstruction of signals with finite rate of innovation in the presence of noise," *IEEE Trans. Signal Process.*, vol. 53, no. 8, pp. 2788–2805, Aug. 2005.
[4] T. Blu, P.-L. Dragotti, M. Vetterli, P. Marziliano, and L. Coulot, "Sparse sampling of signal innovations: Theory, algorithms, and performance bounds," *IEEE Signal Process. Mag.*, vol. 25, no. 2, pp. 31–40, Mar. 2008.
[5] S. Sharma, A. Gupta, and V. Bhatia, "A new sparse signal-matched measurement matrix for compressive sensing in UWB communication," *IEEE Access*, vol. 4, pp. 5327–5342, Aug. 2016.
[6] J. W. Choi, S. S. Nam, and S. H. Cho, "Multi-human detection algorithm based on an impulse radio ultra-wideband radar system," *IEEE Access*, vol. 4, pp. 10300–10309, Sep. 2016.
[7] W. Yin, X. Yang, L. Zhang, and E. Oki, "ECG monitoring system integrated with IR-UWB radar based on CNN," *IEEE Access*, vol. 4, pp. 6344–6351, Sep. 2016.
[8] K.-K. Poh and P. Marziliano, "Compressive sampling of EEG signals with finite rate of innovation," *EURASIP J. Adv. Signal Process.*, vol. 2010, Dec. 2010, Art. no. 183105.
[9] G. Baechler, A. Scholefield, L. Baboulaz, and M. Vetterli, "Sampling and exact reconstruction of pulses with variable width," *IEEE Trans. Signal Process.*, vol. 65, no. 10, pp. 2629–2644, May 2017.
[10] N. A. Baig, M. B. Malik, M. Zeeshan, M. Z. U. Khan, and M. A. Ajaz, "Efficient target detection and joint estimation of target parameters with a two-element rotating antenna," *IEEE Access*, vol. 4, pp. 4442–4451, Aug. 2016.
[11] M. Y. Chua, V. C. Koo, H. S. Lim, and J. T. S. Sumantyo, "Phase-coded stepped frequency linear frequency modulated waveform synthesis technique for low altitude ultra-wideband synthetic aperture radar," *IEEE Access*, vol. 5, pp. 11391–11403, May 2017.
[12] G. Huang, N. Fu, J. Zhang, and L. Qiao, "Sparsity-based reconstruction method for signals with finite rate of innovation," in *Proc. IEEE Int. Conf. Acoust., Speech, Signal Process. (ICASSP)*, May 2016, pp. 4503–4507.
[13] M. S. Kotzagiannidis and P. L. Dragotti, "Sparse graph signal reconstruction and image processing on circulant graphs," in *Proc. IEEE Global Conf. Signal Inf. Process. (GlobalSIP)*, Dec. 2014, pp. 923–927.
[14] G. Huang, N. Fu, J. Zhang, and L. Qiao, "Image reconstruction method of electromagnetic tomography based on finite rate of innovation," in *Proc. IEEE Int. Instrum. Meas. Technol. Conf. (I2MTC)*, May 2016, pp. 1–6.
[15] P. L. Dragotti, M. Vetterli, and T. Blu, "Sampling moments and reconstructing signals of finite rate of innovation: Shannon meets strang-fix," *IEEE Trans. Signal Process.*, vol. 55, no. 5, pp. 1741–1757, May 2007.
[16] H. Olkkonen and J. T. Olkkonen, "Measurement and reconstruction of impulse train by parallel exponential filters," *IEEE Signal Process. Lett.*, vol. 15, pp. 241–244, Feb. 2008.
[17] R. Tur, Y. C. Eldar, and Z. Friedman, "Innovation rate sampling of pulse streams with application to ultrasound imaging," *IEEE Trans. Signal Process.*, vol. 59, no. 4, pp. 1827–1842, Apr. 2011.
[18] K. Gedalyahu, R. Tur, and Y. C. Eldar, "Multichannel sampling of pulse streams at the rate of innovation," *IEEE Trans. Signal Process.*, vol. 59, no. 4, pp. 1491–1504, Jan. 2011.
[19] W. U. Bajwa, K. Gedalyahu, and Y. C. Eldar, "Identification of parametric underspread linear systems and super-resolution radar," *IEEE Trans. Signal Process.*, vol. 59, no. 6, pp. 2548–2561, Jun. 2011.
[20] G. Itzhak, E. Baransky, N. Wagner, I. Shmuel, E. Shoshan, and Y. C. Eldar, "A hardware prototype for Sub-Nyquist radar sensing," in *Proc. Int. ITG Conf. Syst., Commun., Coding (SCC)*, Jan. 2013, pp. 1–6.
[21] E. Baransky, G. Itzhak, N. Wagner, I. Shmuel, E. Shoshan, and Y. Eldar, "Sub-Nyquist radar prototype: Hardware and algorithm," *IEEE Trans. Aerosp. Electron. Syst.*, vol. 50, no. 2, pp. 809–822, Jul. 2014.
[22] G. Huang, N. Fu, L. Qiao, J. Cao, and C. Fan, "A simplified FRI sampling system for pulse streams based on constraint random modulation," *IEEE Trans. Circuits Syst. II, Exp. Briefs*, to be published.
[23] T. K. Sarkar and O. Pereira, "Using the matrix pencil method to estimate the parameters of a sum of complex exponentials," *IEEE Antennas Propag. Mag.*, vol. 37, no. 1, pp. 48–55, Feb. 1995.
[24] G. Zheng, J. Tang, and X. Yang, "ESPRIT and unitary ESPRIT algorithms for coexistence of circular and noncircular signals in bistatic MIMO radar," *IEEE Access*, vol. 4, pp. 7232–7240, Nov. 2016.
[25] P. Stoica and R. L. Moses, *Introduction to Spectral Analysis*. Englewood Cliffs, NJ, USA: Prentice-Hall, 1997.
[26] N. Wagner, Y. C. Eldar, and Z. Friedman, "Compressed beamforming in ultrasound imaging," *IEEE Trans. Signal Process.*, vol. 60, no. 9, pp. 4643–4657, Sep. 2012.
[27] R. G. Baraniuk, "Compressive sensing [lecture notes]," *IEEE Signal Process. Mag.*, vol. 24, no. 4, pp. 118–121, Jul. 2007.
[28] J. A. Tropp and A. C. Gilbert, "Signal recovery from random measurements via orthogonal matching pursuit," *IEEE Trans. Inf. Theory*, vol. 53, no. 12, pp. 4655–4666, Dec. 2007.

[29] H. Zhang, L.-L. Yang, and L. Hanzo, "Compressed impairment sensing-assisted and interleaved-double-FFT-aided modulation improves broadband power line communications subjected to asynchronous impulsive noise," *IEEE Access*, vol. 4, pp. 81–96, Dec. 2016.
[30] W. Huang, Y. Huang, W. Xu, and L. Yang, "Beam-blocked channel estimation for FDD massive MIMO with compressed feedback," *IEEE Access*, vol. 5, pp. 11791–11804, Jun. 2017.
[31] E. J. Candès and M. B. Wakin, "An introduction to compressive sampling," *IEEE Signal Process. Mag.*, vol. 25, no. 2, pp. 21–30, Mar. 2008.
[32] S. Bernhardt, R. Boyer, S. Marcos, and P. Larzabal, "Compressed sensing with basis mismatch: Performance bounds and sparse-based estimator," *IEEE Trans. Signal Process.*, vol. 64, no. 13, pp. 3483–3494, Jul. 2016.
[33] P. Stoica and P. Babu, "Sparse estimation of spectral lines: Grid selection problems and their solutions," *IEEE Trans. Signal Process.*, vol. 60, no. 2, pp. 962–967, Feb. 2012.
[34] D. L. Donoho, Y. Tsaig, I. Drori, and J.-L. Starck, "Sparse solution of underdetermined systems of linear equations by stagewise orthogonal matching pursuit," *IEEE Trans. Inf. Theory*, vol. 58, no. 2, pp. 1094–1121, Feb. 2012.
[35] A. Erdozain and P. M. Crespo, "Reconstruction of aperiodic FRI signals and estimation of the rate of innovation based on the state space method," *Signal Process.*, vol. 91, no. 8, pp. 1709–1718, Aug. 2011.

NING FU received the B.S., M.S. and Ph.D. degrees from Harbin Institute of Technology (HIT), Harbin, China, in 2002, 2004, and 2009, respectively.

Since 2012, he has been an Associate Professor with the Automatic Test and Control Department, HIT. He has published more than 30 journal and conference papers. His current research interests include information acquisition theory, compressive sensing and automatic test technology.

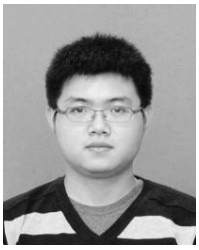

GUOXING HUANG received the B.S. degree from the University of Science and Technology, Beijing, in 2010 and the M.S. degree from Liaoning University, China, in 2013. He is currently pursuing the Ph.D. degree with the Automatic Test and Control Department, Harbin Institute of Technology.

His main research interests include sampling with finite rate of innovation, compressive sensing, and signal processing.

LIYAN QIAO received the B.S., M.S., and Ph.D. degrees from the Harbin Institute of Technology (HIT), Harbin, China, in 1996, 1998, and 2005, respectively.

Since 2009, he has been a Professor with the Automatic Test and Control Department, HIT. He has published more than 40 journal and conference papers. His current research interests include data acquisition technology, mass-storage data record technology, and test information processing.

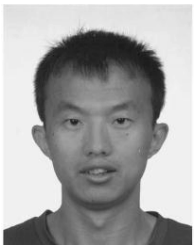

HAORAN ZHAO received the B.S. and M.S. degrees from the Harbin Institute of Technology (HIT), in 2010 and 2012, respectively. He is currently pursuing the Ph.D. degree with HIT.

His main research interests include signal processing, fractional Fourier transform, compressed sensing, and sampling structure.